Escherichia coli maintains pH via the membrane potential

Escherichia coli Maintains pH via the Membrane Potential

Guillaume Terradot, Ekaterina Krasnopeeva,[*] Peter S. Swain,[†] and Teuta Pilizota[‡,§]
School of Biological Sciences, King's Buildings, University of Edinburgh, Edinburgh EH9 3FF, United Kingdom

(Received 18 March 2024; accepted 1 October 2024; published 27 November 2024)

Maintaining intracellular homeostases is a hallmark of life, and *Escherichia coli* works to maintain multiple interconnected electrophysiological variables, such as a near-neutral pH and a sufficient electrochemical gradient of protons, the so-called proton motive force (PMF). To generate the latter, *E. coli* relies on central metabolism to move protons out of the cell, where in its preferred near-neutral extracellular environments this is not enough to achieve reported physiological PMF values. Using mathematical modeling, we predict that *E. coli* also uses proton-ion antiporters for this purpose. Their principal function, powered by the central-metabolism-enabled proton efflux, is to generate the PMF by moving other ions. Consistently, our model predicts that the strength of the PMF sets the maximal rate at which the antiporters work, and so determines the extracellular pH range for which the two homeostases hold. We further predict that artificially collapsing the PMF destroys the membrane potential. In support and by concurrently measuring the PMF and pH in individual cells of *E. coli*, we show that decreasing the PMF's strength impairs the cells' ability to maintain pH and that they have negligible membrane potential when there is no PMF. Finally, we use our model to predict the previously reported ranges of extracellular pH for which *E. coli* expresses three antiporters, by defining their cost through the rate at which they divert protons from generating ATP. Taken together our results suggest a new perspective on bacterial electrophysiology, where cells use antiporters to generate the plasma membrane potential and thus their PMF.

DOI: 10.1103/PRXLife.2.043015

I. INTRODUCTION

Internally, living cells differ from their environment. They typically maintain intracellular homeostases, keeping multiple intracellular variables within a restricted range. For example, cytoplasmic or internal pH (pH_i) is kept close to neutral in organisms across all kingdoms of life [1,2], likely because pH_i affects the stability and function of proteins [3].

However, in unicellular organisms, such as the neutralophilic bacterium *Escherichia coli*, the homeostasis of pH is rarely studied in the context of the other physiological variables that pH influences and the cell regulates, multiple of which are electrical in nature. For example, the electrical potential across the membrane—the membrane voltage $\Delta\psi$—is generated by the charge accumulated at the membrane, which includes protons. This $\Delta\psi$ and the difference between the intracellular and extracellular pH (ΔpH) determine the proton motive force (PMF), the electrochemical gradient of protons. More generally, the electrochemical gradients of all the other ions present in the cell—the ion motive forces (IMFs)—are influenced too by the $\Delta\psi$ and so indirectly by protons. Protons and all other ions can also affect the cells' osmotic pressure Π, which depends on the difference between the extracellular and intracellular concentrations of all the solutes [4].

The intertwined nature of these physiological variables suggests that we should study their maintenance together, even if we wish to understand the homeostasis of one. Building on the pump-leak equations, which are based on decades of experiments on neural and excitable cells [5,6], we develop a mathematical model of bacterial electrophysiology and use it to predict how cells generate their PMF. We note that the low number of intracellular protons necessitated by a near neutral pH_i implies that these protons contribute directly little to the membrane potential. However, central metabolism moves only protons out of the cell, and we demonstrate that cells build a membrane potential using proton-ion antiporters to drive intracellular ion concentrations away from equilibrium. As a consequence, we predict that in alkaline regimes and at zero PMF, cells cannot maintain membrane potential and that the pH_e range over which cells maintain near-neutral pH_i scales with PMF. We measured pH_i during shifts in extracellular pH at two different magnitudes of PMF, as well as the membrane potential at zero PMF. In agreement with the model, we find that cells do not maintain the membrane potential in the absence of PMF and maintain the pH_i at a given pH_e only if the absolute magnitude of PMF is sufficiently high. Together, our results suggest that the primary role of proton-ion antiporters in *E. coli* is to modulate the membrane potential to maintain PMF. This contrasts with their proposed role of directly regulating pH_i by importing or exporting protons depending on the value of pH_i. We do

[*]Present address: Institute of Science and Technology Austria, Am Campus 1, 3400 Klosterneuburg, Austria.
[†]Contact author: peter.swain@ed.ac.uk
[‡]Present address: Department of Physics, Cavendish Laboratory, University of Cambridge, CB3 0HE Cambridge.
[§]Contact author: teuta.pilizota@ed.ac.uk

not exclude a (different kind of) direct pH_i regulation, but we conclude that it should be constrained by the antiporters' role in modulating membrane potential.

II. RESULTS

A. A mathematical model provides an integrated view of bacterial electrophysiology

To describe as simply as possible the interconnected (electro)physiological variables, we developed a minimal mathematical model of bacterial electrophysiology. We consider pH_i, the IMFs, and osmotic pressure, which we define as follows.

For a single ion (x), the electrochemical potential is the free energy required to move an extracellular ion into the cell measured in volts. Mathematically, this potential is

$$\Delta G_x = z_x \Delta\psi + \frac{RT}{F} \ln \frac{[x]_i}{[x]_e} \tag{1}$$

for an intracellular concentration of $[x]_i$ and an extracellular concentration of $[x]_e$. z_x is the valency of the ion, R is the gas constant, T is the temperature, F is Faraday's constant, and $\Delta\psi$ is the membrane potential. We will refer to ΔG_x as the IMF.

A buildup of electrical potential across the membrane—the membrane potential—is enabled by the membrane's hydrophobicity, and, following others [7,8], we assume that the charge accumulated close to the membrane (within a few nm) is equivalent to the surface charge on a parallel-plate capacitor (for a derivation see Ref. [9]). Writing the characteristic capacitance of the bacterial membrane per unit area as C_m, the cell's volume as V, and its surface area as S (see Supplemental Material [10]), we have

$$\Delta\psi = \frac{F}{SC_m} \underbrace{V \sum_x z_x [x]_i}_{Q_i}, \tag{2}$$

where Q_i is the total intracellular charge. Q_i is only nonzero adjacent to the membrane and is equal and opposite in sign to the total extracellular charge Q_e, which is also only nonzero adjacent to the membrane. For simplicity, and without any loss of generality, a rescaling is required otherwise, we assume that the cell has no incompressible volume.

The IMF of particular relevance for *E. coli* is the proton motive force, the PMF or ΔG_{H^+}. A sufficiently high PMF is not only relevant for transport, but also for ATP synthesis via the F_1F_o-ATP synthase and for motility [11]:

$$\Delta G_{H^+} = \Delta\psi - \ln 10 \frac{RT}{F} \Delta\mathrm{pH}, \tag{3}$$

where $\Delta\mathrm{pH} = \mathrm{pH}_i - \mathrm{pH}_e$.

Lastly, bacteria maintain osmotic pressure, Π, within a given range: 0.3–3 atm for *E. coli* [12,13]. It is generated by the difference in total concentration of all solutes across the membrane [8,14], and assuming osmotic coefficients equal to one:

$$\Pi = RT \sum_x ([x]_i - [x]_e). \tag{4}$$

Our model builds on the pump-leak equations developed for excitable cells [5,6] as well as on our previous work [15]. It comprises five species: protons, H^+; hydroxide ions, OH^-; a monovalent cation, C^+; a monovalent anion, A^-; and a lumped species, Y, which includes the contribution to Π and $\Delta\psi$ of all intracellular molecules that are not one of these four ions [Fig. 1(a)]. Examples include charged molecules that cannot cross the plasma membrane (usually referred to as impermeable ions, e.g., free glutamate, the most abundant [16], as well as DNA and RNA) or cross with processes that we do not model. We refer to these molecules as captive molecules because we include a wider definition of Y, not only ions but also neutral solutes. Although we do not specify the anion or the cation, we do assume that the equivalent cation would be uniquely mapped, either as Na^+ or K^+.

All ions except captive ions leak across the plasma membrane [8], but H^+, C^+, and A^- may also be actively transported. To describe how the concentration of C^+ and A^- change we write

$$\frac{d[x]_i}{dt} = -\frac{V_e}{V} \cdot \frac{d[x]_e}{dt} = j_x + \sum_t \sigma_{x,t} j_t, \tag{5}$$

where V_e is the extracellular volume, j_x the flux from leakage, and j_t is the flux from active transport.

Membrane proteins involved in active transport are generally classified as primary, powered by ATP, or secondary, powered by an IMF [17]. Each transporter has a stoichiometric coefficient σ_t that gives the number of molecules or ions transported into or out of the cell. Consequently, the stoichiometric ratio is the ratio of the number of molecules or ions transported into the cell to the number transported out. For example, a proton antiporter with a stoichiometric ratio of two imports two protons per one exported cation; an ATP-driven pump with a stoichiometric ratio of half exports two cations per ATP molecule. Note that we keep V_e and V constant, which we can show does not change our conclusions (see Supplemental Material [10], where we also discuss the requirements for including bacterial volume regulation).

For the intracellular concentrations of protons and hydroxide ions, we include the self-ionization of water at a rate j_w (see Supplemental Material [10]):

$$\frac{d[\mathrm{H}^+]_i}{dt} = j_{\mathrm{H}^+} + \sum_t \sigma_{H^+,t} j_t + j_w \tag{6}$$

$$\frac{d[\mathrm{OH}^-]_i}{dt} = j_{\mathrm{OH}^-} + j_w. \tag{7}$$

Although the dependency of the membrane potential on both the flux from active transport and the leakage through the membrane have been measured in excitable cells and their mitochondria [18–21], we are unaware of such measurements in bacteria. We therefore use a generic form for their dependency on the ΔG of the transport reaction [22]:

$$j = j^+ \left(1 - e^{\frac{F}{RT}\Delta G}\right), \tag{8}$$

where the transport mechanism, such as the number of intermediate steps involved, determines the rate j^+ [8]. Like others, we assume that j^+ is constant for active transport at steady state [6,7]. For leakage, we use an expression that

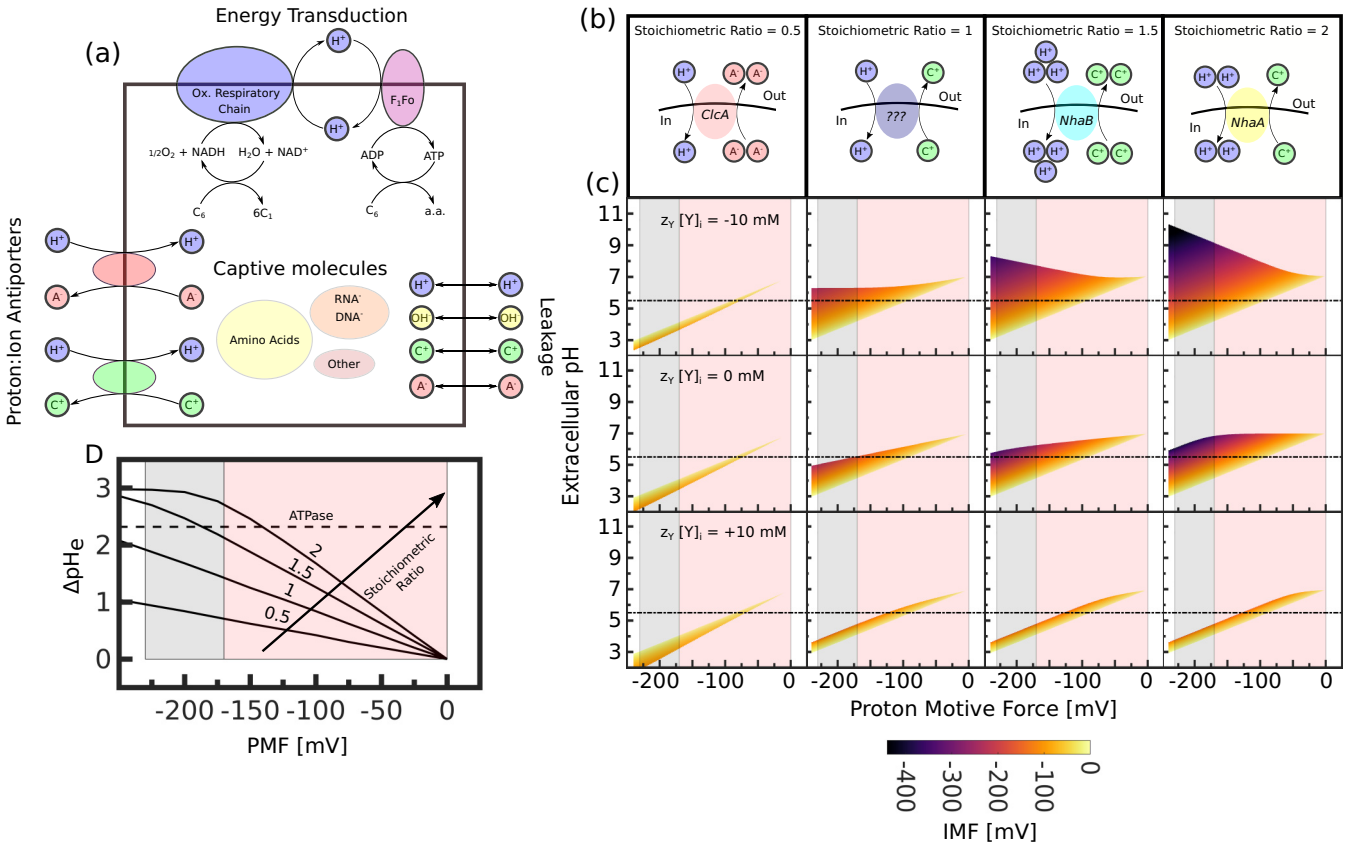

FIG. 1. Our mathematical model of *E. coli's* electrophysiology predicts that the pH_e range over which cells can maintain a neutral pH_i is directly related to the PMF. (a) A simplified model of *E. coli*'s electrophysiology. We distinguish two classes of chemical species contributing to the membrane potential: small ions, which both leak and are pumped across the membrane, and captive molecules, which include both ions that cannot cross the membrane and molecules that might be pumping by processes we do not explicitly model. Only two cations, protons and a representative cation C^+, and two anions, hydroxide ions and an anion A^-, are included. Metabolic reactions that generate PMF are either the electron transport chain or the F_1F_o ATPase. We fix the concentrations of NADH, NAD^+, ATP, and ADP, and of extracellular ions. Proton-ion antiporters exchange protons for C^+ or A^- and generate ion motive forces. (b) We consider four antiporters. Their stoichiometric ratio is the ratio of the number of protons to the number of ions exchanged. (c) We plot the possible steady-state solutions for each antiporter for a given PMF between -240 and 0 mV, a pH_i of 7, and pH_e between 2 and 12. Extracellular $[CA]_0 = 100$ mM, and we consider three values of total captive molecules, $z_Y Y_i$. The horizontal black line marks $pH_e = 5.5$. Gray and red shading shows values of the PMF expected for the respirative and fermentative regimes (see Supplemental Material [10] for estimates of these values). The color scale indicates the ion motive force (IMF). (d) The pH_e range (difference between maximum and minimum pH_e) over which $pH_i = 7$, is plotted as a function of the PMF for antiporters of different stoichiometric ratio (indicated with an arrow). Extracellular $[CA]_0 = 100$ mM and $z_Y Y_i = 0$ mM.

depends on the membrane's permeability and is derived from measurements on mitochondria [20] (see Supplemental Material [10]).

We first note that without active transport, ions will leak across the membrane, making $\Delta G_x = 0$. However, the membrane potential will not vanish because of the captive molecules that are charged. This equilibrium $\Delta\psi$, or Donnan potential, cannot reach physiological levels without generating an excessive Π (Fig. S1 [10]). To generate both a physiological $\Delta\psi$ and Π, cells must actively transport ions.

Second, by considering four possible scenarios of active transport, either anions or cations either in or out (Fig. S2 [10]), we see that for the near neutral pH_i only exporting cations robustly generates both physiological $\Delta\psi$ and Π. Exporting anions results in positive $\Delta\psi$, making it a viable strategy only in a narrow range of acidic extracellular environments. Moving ions into the cell produces values of Π outside the experimentally observed range, e.g., at $\Delta\psi = -150$ mV, osmotic pressure is above 500 atm. This is because the total number of intracellular ions needed to achieve the same charge concentration difference, i.e., $\Delta\psi$, is different. For example, for negative $\Delta\psi$ when the cell pumps in anions, cations will passively leak in too, with their intracellular concentration exponentially increasing with more negative $\Delta\psi$. When the cell pumps out cations, however, the more negative $\Delta\psi$ causes fewer and fewer anions to leak in, giving a smaller Π (see Supplemental Material [10]). These conclusions hold too if we allow both anions and cations to be pumped simultaneously, Fig. S3.

Third, we include the following active transport reactions. Cell metabolism powers protons export by oxidising NADH or hydrolysing ATP [23]. We refer to these two regimes as respirative and fermentative. However, at a near neutral pH_i and given the small volume of a typical *E. coli* cell, the

concentrations of protons and hydroxide ions are too low to contribute substantially to $\Delta\psi$. For example, if we take length to width ratio as 3:1, where width is 1 μm (see also Supplemental Material [10]), even if pH_i is in the 6–8 range, the extremes for most cells [1,24], $[H^+]_i$ and $[OH^-]_i$ contribute to $\Delta\psi$ at most ± 3.5 mV (see also Fig. S4 [10] for the error on $\Delta\psi$ if we disregard the contribution of $[H^+]_i$ and $[OH^-]_i$ across a range of conditions). We, therefore, assume that the cell reimports these protons to export other ions and thus generates reported values of $\Delta\psi$ that in some conditions have been measured to go all the way down to -200 mV [25]. We further assume the cell exports these ions through proton-ion antiporters, because the intracellular concentrations of other ions are much less restricted and because no other types of cation (apart from proton) exporters, such as ATP-driven, are known to exist in *E. coli*.

Finally, we assume that cells maintain a nonzero value of the PMF. Recent observations of *E. coli*'s motor and swimming speeds show not only a nonzero but also a constant value for growth rates as low as 0.4 h^{-1} [26,27], indicating that the cells likely maintain the value of PMF fixed in a given condition (in Supplemental Material [10] we determine PMF's physiological limits). To do so, while also maintaining a constant, near neutral pH_i, cells must control $\Delta\psi$, modifying its value in response to changes in pH_e.

B. The cell's PMF determines the range of pH_e at which it maintains near neutral pH_i

In our model, metabolism powers the export of protons. To generate a physiological $\Delta\psi$, and thus PMF, cells change the concentrations of other ions only through the action of antiporters.

To find a unique signature of this mechanism of generating PMF, i.e., using proton-ion antiporters that are themselves powered by the PMF, we examine how the PMF's magnitude influences pH_i. We look at four types of antiporters [Fig. 1(b)], three of which have identical stoichiometric ratios to antiporters in *E. coli*: ClcA [28], NhaB [29], and NhaA [30]. The fourth, which we depict with question marks, is a hypothetical transporter that exports one cation for one proton.

Although changes in pH_e may generate a change in expression of the antiporters or changes in their stoichiometric ratios [31,32], we include such effects only implicitly in the value of j^+ in (8). This value once positive is not critical for much of our analysis.

The reaction powered by the antiporter a in (5) is

$$\sigma_{H^+,a}\,H_e^+ + \sigma_{x,a}\,x_i \rightleftharpoons \sigma_{H^+,a}\,H_i^+ + \sigma_{x,a}\,x_e. \tag{9}$$

For this antiporter to use the proton gradient across the plasma membrane to export ions and so simultaneously generate physiological $\Delta\psi$ and Π (as discussed in Fig. S2 [10]), this reaction's ΔG should be negative:

$$\Delta G_{x,a} = \sigma_{H^+,a}\,\Delta G_{H^+} - \sigma_{x,a}\,\Delta G_x < 0, \tag{10}$$

where ΔG_x satisfies Eq. (1).

At steady state, the leakage of x back across the membrane balances this export, implying that the leakage flux j_x must be positive and, from (8), have $\Delta G_x < 0$. Combining with (10) implies:

$$\frac{\sigma_{H^+,a}}{\sigma_{x,a}}\Delta G_{H^+} < \Delta G_x < 0 \tag{11}$$

and the IMF, ΔG_x, is bounded. The two limits correspond to the antiporter working maximally when ΔG_x is most negative or negligibly when ΔG_x is zero.

Given (11), and for a given antiporter characterized by its stoichiometric ratio $\sigma_a = \frac{\sigma_{H^+,a}}{\sigma_{x,a}}$, we wish to determine the range of steady states that the antiporter can support. To do so, we fix the concentrations of extracellular ions, pH_e, and the charge and intracellular concentration of the captive molecules. We then assume that pH_i is neutral, and specify a steady state by the value of the PMF. If an antiporter can maintain this steady state, then (11) must hold.

To check if (11) is valid, we should determine ΔG_x. First, we find the membrane potential, simplifying (2) to:

$$\Delta\psi \simeq \frac{FV}{SC_m}(z_Y[Y]_i + [C^+]_i - [A^-]_i) \tag{12}$$

by ignoring the negligible contributions of protons and hydroxide ions. Second, we use (1) to include the known extracellular concentrations, which we can assume the cell's actions leave unchanged:

$$\Delta\psi \simeq \frac{FV}{SC_m}\Big(z_Y[Y]_i + [C^+]_e\,e^{\frac{F}{RT}(\Delta G_{C^+}-\Delta\psi)} - [A^-]_e\,e^{\frac{F}{RT}(\Delta G_{A^-}+\Delta\psi)}\Big). \tag{13}$$

Third, the antiporter pumps only one of these ions. The other leaks passively across the membrane and has a ΔG of zero at steady state. Equation (13) then reduces to an equation for a given ΔG_x. We solve this equation and evaluate (11).

The result is that the antiporters with different stoichiometries generate steady states with $pH_i = 7$ for different ranges of PMF and pH_e [Figs. 1(c), S5, and S6].

For cation-exporting antiporters, such as NhaA and NhaB, the lower limit of pH_e that supports a steady state is determined by the upper bound of (11). When pH_e decreases below pH_i for a constant PMF, the cell generates a more positive membrane potential to maintain the PMF, see (3). For cation-exporting antiporters, which work to build negative $\Delta\psi$ and so negative ΔG_{C^+}, weaker pumping antiporters that allow cations to build up, decreasing the magnitude of ΔG_{C^+}, are necessary. At the minimal possible pH_e, the pumping by the antiporters is negligible, and the magnitude of ΔG_{C^+} is close to zero. For these antiporters, the upper bound of (11) determines the lower limit of pH_e. When pH_e increases above pH_i for a constant PMF, the cell generates a more negative membrane potential to maintain the PMF. Cation-exporting antiporters pump more strongly, decreasing $\Delta\psi$ and increasing the magnitude of ΔG_{C^+}. At the maximal possible pH_e, the antiporter builds ΔG_{C^+} and $\Delta\psi$ to the maximal magnitudes it can, and $\Delta G_{C^+} = \sigma_a \Delta G_H$.

Alternatively, for ClcA-like antiporters, which use the PMF to generate a more positive $\Delta\psi$ by exporting anions, it is the lower bound of (11) that sets the lower limit of pH_e. At this bound, the antiporters increase $\Delta\psi$ by exporting anions as much as they can, and the absolute ΔG_{A^-} is maximal. Note that the antiporters import protons to generate this response

even though the extracellular environment is acidic. They do not need to export protons to raise pH_i directly as previously proposed [1,33]. The upper bound of (11) sets the upper limit of pH_e. The antiporters generate the more negative $\Delta\psi$ needed by more weakly exporting anions.

Our argument holds for all values of σ_a, including those for electroneutral antiporters. The transporters' electrogenicity is unimportant, rather it is their ability to use the PMF generated by the central metabolism to move ions, out of the cell. The invested PMF to do so will be regenerated by the central metabolism (at different rates in different pH_e) allowing electroneutral antiporters to change intracellular ion concentrations sufficiently to manipulate $\Delta\psi$.

The range of pH_e over which the cell maintains a steady state with $pH_i = 7$ scales with the value of the PMF maintained, increasing if the PMF is more negative for all the antiporters we tested (Fig. 1(d); see also discussion in Supplemental Material [10]). A more negative PMF has two advantages: it increases the free energy available to power the antiporters, increasing the maximal flux at which they can work and extending the lower bound of (11); and it increases the $\Delta\psi$ at neutral pH_e when ΔpH is zero, decreasing ΔG_x farther away from its maximal value of zero.

We therefore predict that cells can maintain pH_i over the widest range of pH_e in the respirative rather than the fermentative regime because the PMF is then more negative [Fig. 1(d)]. This robustness to pH_e comes at a cost. A more negative PMF will require the electron transport chain to export protons at a greater rate because the correspondingly more negative membrane potential will increase the import rate of protons by both the antiporters and leakage.

In contrast, for a hypothetical ATP-driven cation efflux pump, some mammalian cells generate $\Delta\psi$ using a sodium-potassium ATPase [34], these observations would not hold. Like before, the ΔG of such pumping reaction should be negative and the reaction balanced by leakage at steady state, implying:

$$\frac{\sigma_{\mathrm{ATP},t}}{\sigma_{x,t}}\Delta G_{\mathrm{ATP}} < \Delta G_x < 0, \tag{14}$$

where the stoichiometric ratio describes the number of ions exported per number of ATP molecules. The free energy of ATP hydrolysis rather than the PMF determines the lower bound of ΔG_x, and so the range of pH_e at which cells may keep pH_i near neutral is independent of the PMF, Fig. S7 [10].

C. At pH_e 5.5, *E. coli* maintains pH_i if the PMF is sufficiently negative

To confirm the PMF's predicted role in determining the robustness of pH_i, we should measure PMF and pH_i simultaneously in individual cells while controlling the magnitude of the PMF. We can do so by using the speed of the bacterial flagellar motor to indicate PMF and a ratiometric pH sensor (pHluorin [35]) to measure pH_i [15,36,37].

The bacterial flagellar motor is a rotary nanomachine [11], and its speed is proportional to the PMF in *E. coli* [25,38,39] (Fig. S8 [10]). Measuring changes in the motor's speed is therefore equivalent to measuring changes in the PMF. By attaching a cell to the surface of a cover slip [40] and a plastic bead to a genetically modified filament stub of the flagellum [36,37,41–43], we are able to measure the rotation of the motor labeled with the bead through placing the bead in a heavily attenuated optical trap and performing back-focal-plane interferometry [Fig. 2(a)] [44,45]. The strains we use also express cytoplasmic pHluorin [15,36,37].

To change the PMF, we used a sealed tunnel-slide configuration [36,43,46]. Cells are kept in a potassium phosphate buffer containing glucose and sufficient NaCl to match the osmolality of the growth media. They eventually run out of oxygen, at which point the magnitude of the PMF drops [47] [Fig. 2(b)]. Although the timing of the drop varies between 20 and 30 min and depends on the concentration of cells on the tunnel-slide surface, as has been found too for swimming cells [47], there is a conserved, characteristic steplike shape (Fig. S9 [10]).

We changed pH_e from 7.0 to a lower value (4.3–6), using a mixture of organic acids, and observed pH_i, first at a higher absolute PMF, which cells maintain in the presence of oxygen, and then at lower one when the oxygen in the tunnel slide runs out [arrows in Fig. 2(b)] . The motor's speed, and hence the PMF, changed in these aerobic and anaerobic conditions [Figs. 2(b) and 2(c), Fig. S11].

As predicted [Figs. 1(c) and 1(d)], cells maintain near-neutral pH_i (between pH 7 and 8) over a wider range of pH_e for the higher magnitude PMF [compare aerobic and anaerobic conditions in Figs. 2(c) and 2(d)]. In Fig. S10 [10] we plot both the data and the pH_e range predicted by the model, ΔpH_e, over which cells maintain pH_i near neutral to explicitly test the importance of the antiporters in the model. We do so for the NhaA-like antiporter and a putative ATP-driven ion export pump. Only the data and the response for the NhaA-like antiporter show a dependency of ΔpH_e on PMF.

Although the predictions in Fig. 1(c) are for steady states, we can also monitor transitions between these steady states in our experiments. For example, changing pH_e to 5.5 temporarily acidified the cytoplasm [Fig. 2(c)], but pH_i then recovered towards its initial value providing the magnitude of the PMF was kept high by oxygen [Fig. 2(e)]. As oxygen fell and the PMF's magnitude dropped, pH_i returned to the value seen when pH_e was first changed. If we altered pH_e to below 5, we observed no dynamic recovery, and both the magnitude of the PMF and pH_i dropped permanently, indicating that the gradient of protons across the membrane had likely collapsed (Fig. S11 [10]).

D. A ΔpH requires a PMF if antiporters generate the membrane potential

Another prediction of our model is that cells require a PMF to maintain a $\Delta\psi$. Without a PMF the antiporters cannot drive the membrane potential from equilibrium, and so if their role is to generate $\Delta\psi$, both $\Delta\psi$ and ΔpH should individually be zero when the PMF is zero, rather than only their weighted sum. Figures 3(a) and 3(b) show that for antiporters with different stoichiometric ratios, 0.5, 1.5, and 2 as examples, our model does predict that both vanish, although $\Delta\psi$ is not exactly zero because the captive charges prevent the equilibrium $\Delta\psi$ from being zero.

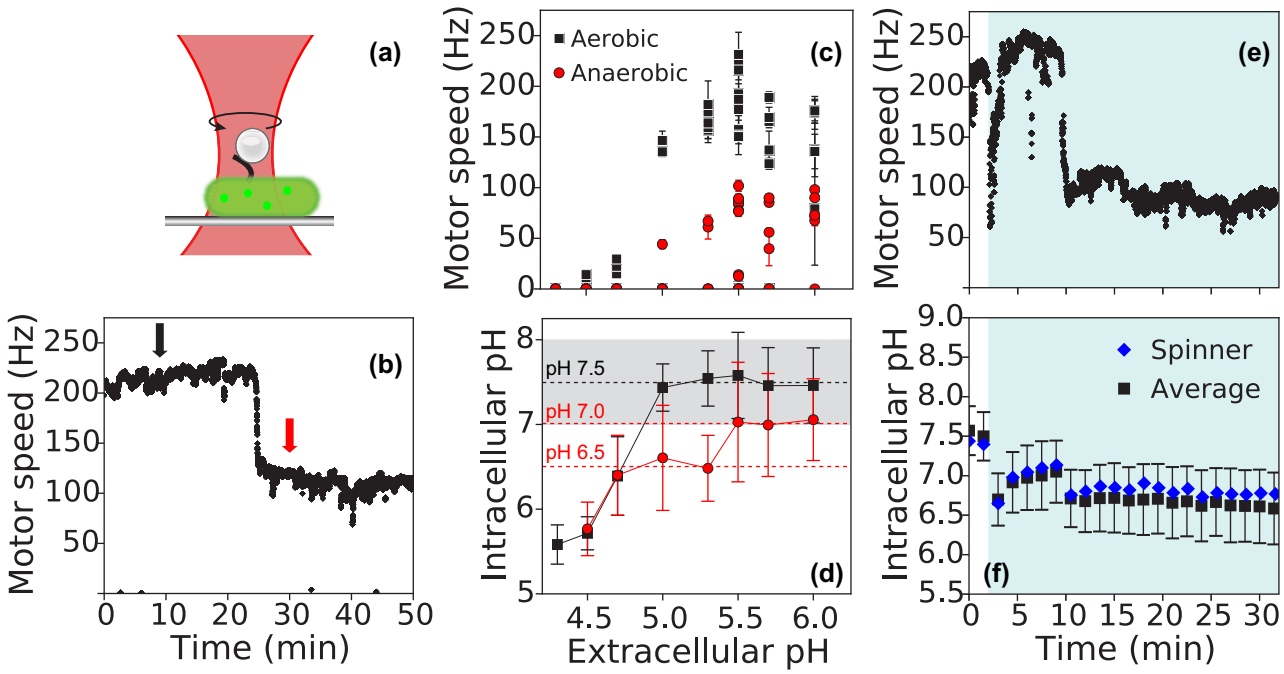

FIG. 2. At acidic pH_e, *E. coli* maintains a neutral pH_i if the magnitude of the PMF is sufficiently high. (a) A schematic showing *E. coli* immobilized on a glass coverslip with a polystyrene bead attached to a sticky stub of a bacterial flagellar filament. We placed a bacterium in the focus of a heavily attenuated, sharply focused laser to detect the position of the bead at high speeds and used the flagellar motor's rotational speed as a proxy for PMF. The cell's cytoplasm is in green to illustrate that we concurrently monitored a fluorescent pH sensor. (b) An example of the motor speed of a single cell in a sealed tunnel slide at $pH_e = 7.0$ with 20 mM glucose. The sharp drop at ∼25 min occurred when oxygen was exhausted. The arrows show where we measured aerobic (black) and anaerobic (red) speeds. (c) Motor speeds obtained from individual cells plotted as a function of pH_e. We calculated each motor's speed as the mean of a ± 45 s interval around the two time points indicated in (b). The error bars are standard deviations. Total number of motors, and so cells, included is 59. (d) pH_i changes plotted against pH_e, where the values of pH_i are the mean of 90–316 cells for the time points indicated in (b); error bars are standard deviations. Gray shading shows the near neutral pH_i region, between pH 7 and 8. (e) An example of a single-cell motor speed upon shifting to $pH_e = 5.5$, indicated by blue shading. Initially, cells were at $pH_e = 7$, and then we shifted pH_e to 5.5 at $t = 2$ min (blue shade) and sealed the tunnel slide. The sharp drop in speed at the point where pH_e changed is a loss of signal rather than a true change: the bead, rotated by the motor, moved out of the laser's region of detection due to flow. (f) The dynamics of pH_i for the cell whose PMF is given in (e). Blue diamonds show the cell from (e); black squares show the mean and standard deviation of that, as well as all the other cells in the field of view (∼30).

If the cells had an ATP-driven efflux pump, however, they could generate a membrane potential with no PMF, with $\Delta\psi = \ln(10)\frac{RT}{F}\Delta\text{pH}$ [Fig. 3(b), far right]. For example, fluctuations in $\Delta\psi$ can be measured from ΔpH in erythrocytes in the presence of a protonophore [48,49].

We therefore tested whether *E. coli* cells can generate $\Delta\psi$ when their PMF is collapsed. We treated cells with 100 μM carbonyl cyanide m-chlorophenylhydrazone (CCCP), a commonly used protonophore [50,51], in alkaline medium [Fig. 3(c)], where the predicted difference between the antiporters and putative ATP-drive efflux pumps is most notable [Fig. 3(b)]. Changing pH_e to either 8.15 or 8.45 decreased the PMF, and it was now composed mostly of $\Delta\psi$, with ΔpH close to zero. If the cells maintain such $\Delta\psi$ when PMF = 0, we would then expect to see a significant ΔpH. However, when we added CCCP, the PMF dropped to zero and importantly ΔpH was also zero, in agreement with the antiporter model and indicating from Eq. (3) that the cells no longer maintained their membrane potential. In Fig. S12 [10] we experimentally confirmed that a sufficient amount of intracellular ATP was available to power any potential ATPases for ∼10 min after we added CCCP. The recovery of pH_i we observed upon the alkaline shift [Fig. 3(c)] agrees with previous measurements [52]. If we estimate $\Delta\psi$ using the known range of the PMF during respiration on glucose, $\Delta\psi$ stays approximately constant during the alkaline shift (Fig. S13 [10]), supporting a reported ∼10 mV change [52]. Nevertheless, and as expected in the antiporter model, $\Delta\psi$ is negligible in the absence of PMF [Figs. 3(c) and 3(d)].

E. The optimal choice of antiporter depends on extracellular pH

We can use our model to predict when cells should express each type of antiporter. For a given PMF and pH_e, multiple different antiporters are able, in principle, to maintain the same steady state [Fig. 1(c)], and a cell could express or up-regulate the expression or activity of a preferred antiporter [31,32]. To identify preferred antiporters, we estimate the energetic cost of each.

We define this cost as the total flux of protons into the cell by both the antiporters and leakage. They are costly, by this definition, because they are not directly involved in the generation of ATP. In the respirative regime, their import,

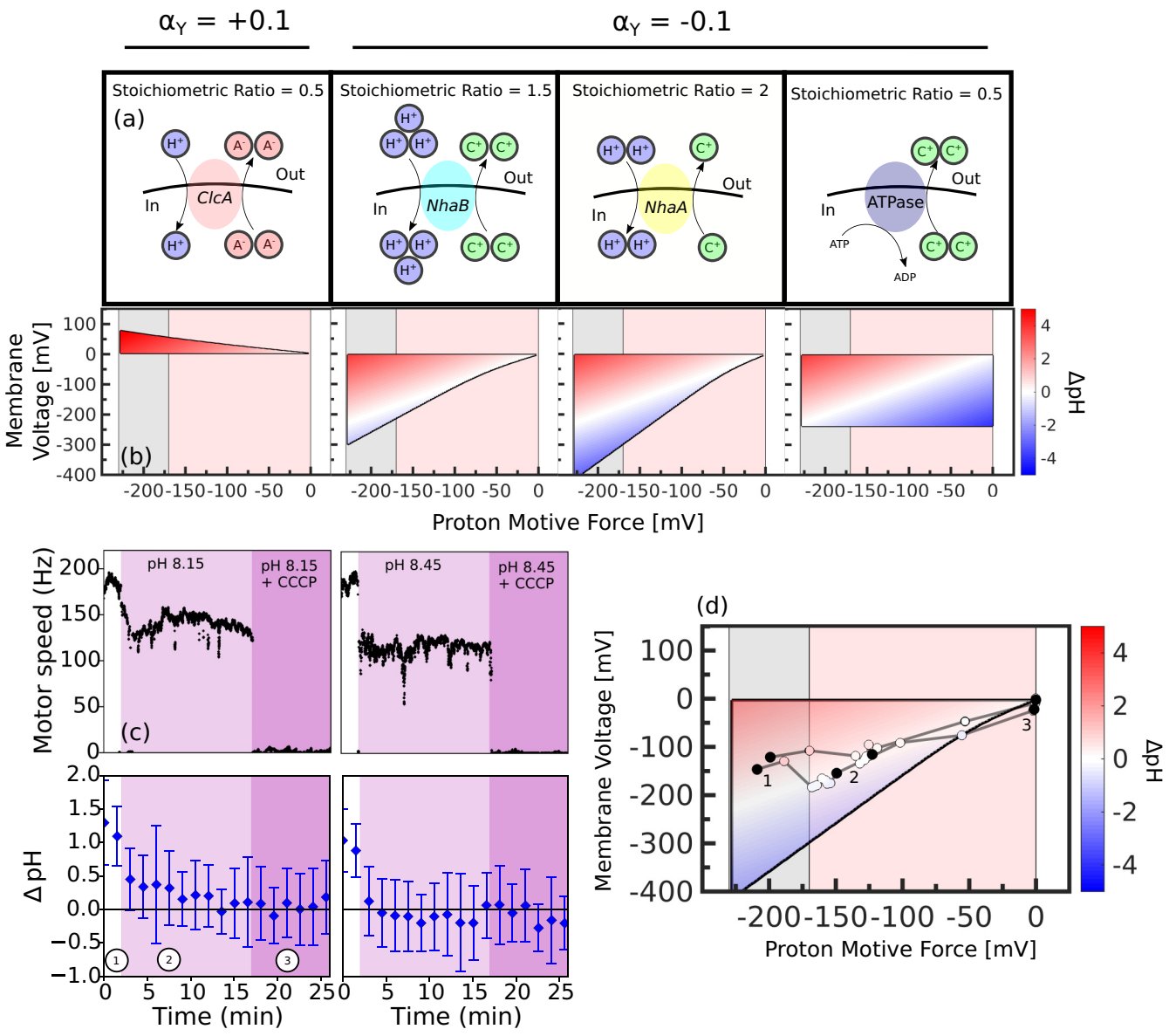

FIG. 3. Collapsing the PMF gives results consistent with proton antiporters generating *E. coli*'s membrane potential. (a) Schematics of the ion pumps in the model. We include a hypothetical ATPase with a stoichiometry of one ATP per two cations and antiporters with three different σ_a. (b) Generating $\Delta\psi$ by an antiporter or by an ATPase gives a different $\Delta\text{pH} = \text{pH}_i - \text{pH}_e$ when the PMF is close to zero. We plot the possible steady-state membrane potentials as a function of the PMF and show ΔpH using the color scale with $\text{pH}_i = 7$ (blue is alkaline pH_e; red is acidic). The anionic antiporters maintain a positive potential; the cationic antiporters maintain a negative potential. For computational reasons, we show an approximate $\Delta\psi$ (with an error of ∼10 mV, Fig. S4 [10]). (c) The single-cell motor speed (top panels), reporting on the PMF, and the average ΔpH (bottom panels) upon alkaline shifts to 8.15 (first column) or 8.45 (second column) followed by addition of a protonophore, CCCP, support a $\Delta\psi$ generated by antiporters. We changed pH_e from 7 (white, annotated 1) to above 8 (pink, annotated 2) and then added CCCP (purple, annotated 3). ΔpH is the mean of ⩾30 cells; errors are standard deviations. (d) To demonstrate that the data qualitatively agree with the model's prediction of a vanishing membrane potential we plot it against the model prediction of membrane potential versus the PMF for NhaA-like antiporter in (b). Motor speed and pH_i data obtained in (c) are converted to PMF and $\Delta\psi$ (white circles) as follows. For each pH_i measurement time point, we take the motor speed interval ±45 s and average it. Correspondingly, the first and last time points are only 45 s intervals. To get the PMF value from the averaged motor speed we use the conversion factor of 1.13 mV/Hz (Fig. S13 [10]), and to get the $\Delta\psi$ from that PMF we use (3). Black circles correspond to the three regimes indicated with numbers 1, 2, and 3 in (c). The gray and red shading indicates the respirative and fermentative regimes.

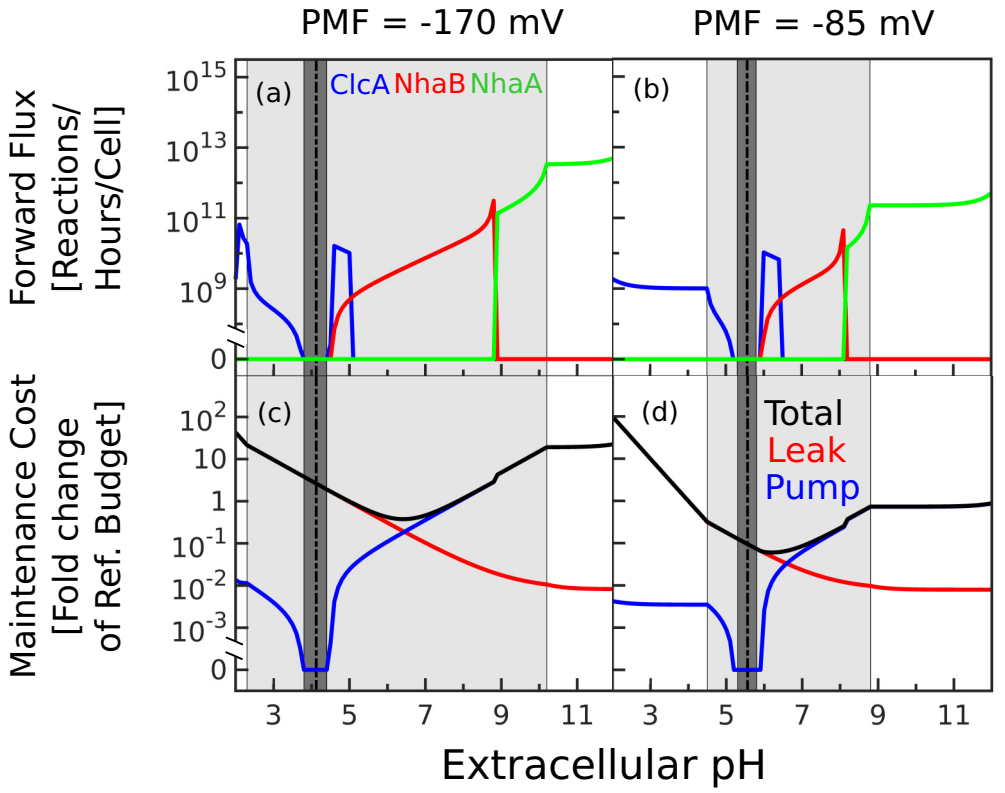

FIG. 4. Maintaining pH_i, the PMF, and osmotic pressure at minimal cost predicts a homeostatic strategy for *E. coli* across different pH_e. We maintain pH_i as close as possible to 7, $-10 \leqslant z_Y \leqslant 10$, and set the osmotic pressure to 1 atm and the extracellular $[CA]_0$ to 50 mM. The black dotted line marks the pH_e for which $\Delta\psi = 0$; to the left, $\Delta\psi > 0$; to the right, $\Delta\psi < 0$. The dark gray indicates where the optimal solution has $\Delta G_{C^+} = \Delta G_{A^-} = 0$ and therefore requires no antiporters. The light gray area indicates where pH_i can be maintained exactly at 7; on the left, $pH_i < 7$; to the right, $pH_i > 7$. (a), (b) For two choices of the PMF, we show the antiporter and its flux that minimises (15) for different pH_e: a ClcA-like antiporter is in blue, a NhaB-like one in red, and a NhaA-like one in green. The transition between NhaB to NhaA to the right, i.e., when $\Delta\psi < 0$, is sudden because at sufficiently negative $\Delta\psi$ NhaB starts working in the opposite direction. In the same regime, $\Delta\psi < 0$, and when the pH is kept exactly at 7 (light gray area), there is a regime where ClcA and NhaB are equally costly. (c), (d) For the same PMFs, we show the minimal cost (black) in protons per cell per hour relative to a reference budget, which we estimate for *E. coli* doubling every 60 min aerobically in minimal medium supplemented with glucose (see Supplemental Material [10]). We also show the contributions to the cost of the antiporters' activity (blue) and of leakage (red).

unlike that through the F_1F_o ATPase, does not generate ATP; in the fermentative regime, they are costly because they undermine F_1F_o's ATP-driven export of protons. We consider three antiporters, all with equivalents in *E. coli* [Fig. 1(b)], and write the cost as

$$\text{Cost} = j_{H^+} + \sum_a \sigma_{H^+,a}\, j_a, \tag{15}$$

where as before the flux from leakage is j_{H^+} and from an antiporter a is j_a.

The cost of maintaining a given PMF is minimised by using the antiporter with the smallest value of $\sigma_{H^+,a} j_a$, where (8) and (11) determine the value of j_a (see Supplemental Material [10]). The result is that for a minimal cost, cells should use one type of antiporter for a specific range of pH_e [Figs. 4(a) and 4(b)]: the ClcA-like antiporter in a pH_e between approximately 2 and 5; the NhaB-like antiporter between 5 and 9; and the NhaA-like one between 9 and 12. Consistently, ClcA is important at acidic pH [53] and NhaA in alkaline pH [30,54,55], with its activity increasing once pH_e goes above 6.5 [56].

As pH_e changes so too does the dominant factor in the cost. For an alkaline pH_e, the antiporters dominate the minimal cost; at acidic pH_e, the leakage of protons dominates [Figs. 4(c) and 4(d)].

When minimizing the cost, we also optimize the concentration and valency of the captive charges. For a small range of pH_e, the cost is minimized by generating $\Delta\psi$ from the captive charges alone (Fig. 4), but only near equilibrium and so likely physiologically irrelevant. The optimal valency of the captive charges alters sign as pH_e changes (Fig. S14 [10]) and should be positive for sufficiently acidic pH_e. This prediction is consistent with cells responding to acidic stress by generating positive charge: they convert some amino acids into more positively charged molecules and negatively charged glutamate into neutral γ-aminobutyric acid [57–59].

III. DISCUSSION

How bacteria maintain homeostasis has long been of interest. Here we gain new insights by exploring the consequences of protons and hydroxide ions that contribute little to the membrane potential at a near-neutral pH_i. We identify that active

export of other ions is necessary for homeostases, and, with no evidence for ATP-driven cation efflux in *E. coli*, we predict that proton antiporters generate the cell's out-of-equilibrium membrane potential. As a consequence, the PMF, which powers these antiporters, is necessary to maintain ΔpH and $\Delta\psi$. Further, the PMF determines how robustly cells can maintain their pH_i for different pH_e. We confirmed this prediction by demonstrating that collapsing the PMF depolarised *E. coli* cells (Fig. 3) and that a lower magnitude PMF impaired their maintenance of pH_i (Fig. 2).

Our results suggest that we may reconcile contradictory observations on the dynamics of pH_i, [60–62] and [24,63] reproduced in Fig. S15 [10], if the cells in each experiment had different PMFs, perhaps because in one oxygen was present, and the other not.

Our prediction that proton-ion antiporters regulate $\Delta\psi$ suggests a shift of perspective away from electrogenicity, or the net amount of charge transferred by an antiporter, to its stoichiometric ratio. If antiporters only through their transport of protons keep pH_i neutral and $\Delta\psi$ fixed as previously thought, the cell would lose control of the PMF as pH_e changes. Importantly, cells would also need some other cation efflux pumps, in addition to those for protons, to change ion concentrations to generate physiological $\Delta\psi$. In our perspective, even an electroneutral antiporter can generate $\Delta\psi$ because it moves an ion out for proton in, where the cell's metabolism then works to export the protons imported by the antiporter. Similarly, at low extracellular pH, ClcA, rather than exporting protons to raise pH_i, exports chloride ions to generate $\Delta\psi$ [Figs. 1(c), 1(d)] and metabolism exports the protons it imports. Alternatively, cells could actively maintain chloride motive force or actively import cations, such as by potassium ATPases [64], but we expect that the more likely strategy is to export anions so as to keep the osmotic pressure in check (see Supplemental Material [10]). For example, active chloride export occurs in the acidophile *Bacillus coagulans* [65].

This change of perspective applies too to alkalinophiles, which maintain a more negative $\Delta\psi$ compared to neutralophiles [1] and often have proton-sodium antiporters [66]. If those antiporters are responsible for generating the plasma membrane potential as we suspect, then we predict that their distinctive characteristic should be a high proton-to-sodium stoichiometric ratio.

Our work has caveats. It neither predicts the preferred pH_i nor addresses how cells recover this pH_i after a change in pH_e but rather determines whether a steady state with a neutral pH_i is possible. Therefore, we have ignored the complexity of how cells regulate the activity and expression of antiporters as they make this transition [31,32]. Any direct regulation, which we do expect not only because our model does not predict the preferred pH_i but also because antiporters activity and expression of antiporters are known to be pH_i regulated [31,32], will be subject to the role of the antiporters in the maintenance of $\Delta\psi$.

The model is deliberately simple to be clear, focusing on one type of cation and one type of anion, both with a single charge. Multiple types of ions are of course present, but our approach remains qualitatively valid if cells regulate the membrane potential principally through one type of cation or anion whose active transport is dominated by one type of antiporter. We only implicitly include chemical reactions that modify pH_i, such as the decarboxylation and carboxylation of amino acids and their transport [31,57], by changing the valency and concentration of captive molecules and so undoubtedly miss much [31]. Finally, our modeling excludes bacterial cell volume regulation. We expect this regulation to change the predicted values of $\Delta\psi$ and PMF, but not Eqs. (11) and (14).

Moving away from bacteria, proton-ion antiporters are widespread, and defects in these antiporters in mammalian cells are associated with disease [67–69]). In mammals, the members of the NHE gene family, to which *NhaA* belongs, and the CLC gene family, to which *ClcA* belongs, are also thought to help maintain cytoplasmic pH [70,71]. Nevertheless, the multiple compartments of eukaryotic cells may mean that sustaining a PMF between the cytoplasm and extracellular space is not under such strong selection, constraining the activity of proton-ion antiporters less.

IV. METHODS

A. Strains and media

For simultaneous measurements of pH_i and the single-cell motor speed we use two strains of *E. coli*. The first is a derivative of MG1655 (EK07 [36]) with sticky filaments and chromosomal expression of pHluorin. The second is the AB1157 strain [47] modified to carry the sticky flagellin encoding gene $fliC^{sticky}$ [36,41] and transformed with pkk223-3-pHluorin (M153R) plasmid [35]. $FliC^{sticky}$ makes filaments hydrophobic so that they readily stick to polystyrene beads [41]. With the two strains, we confirmed that there are no significant strain-to-strain differences in the behavior we observe. We used strain EK07 for $pH_e = 5.5$ experiments; strains EK07 and AB1157 for a pH_e of 5.7 and 6.0; strain AB1157 for a pH_e of 4, 4.3, 4.5, 4.7, 5, and 5.3; and strain EK07 for a pH_e of 8.15 and 8.45. MG1655 carrying pWR20-Q7* (Kanamycin resistance) and wild-type MG1655 was used for ATP measurements [72]. Bacteria were diluted ($\times 10^{-3}$) from the frozen overnight culture (OD $\approx$3) and grown in lysogeny broth (LB: 10 g tryptone, 5 g yeast extract, 10 g NaCl per 1 l) in conical flask at 37 °C with shaking (220 rpm).

B. Flagellar motor speed recording and analysis

Cells were harvested at OD = 2.0 to maximize the fraction that expressed the flagellar motor (Spectronic 200E Spectrophotometer, Thermo Scientific, UK). Cells were prepared for microscopy as before [73] using tunnel slides [74]. Experiments were performed in the motility buffer (BMB: aqueous solution of 6.2 mM K_2HPO_4, 3.8 mM KH_2PO_4, 67 mM NaCl, and 0.1 mM EDTA, pH 7.02) supplemented with 20 mM glucose.

For aerobic-anaerobic shifts [Figs. 2(b) and S9], cells were kept in glucose-supplemented BMB in the tunnel slide, where fresh BMB was flushed in just prior to the recording and the slide was sealed with CoverGrip™ Coverslip Sealant (Biotium, USA) to prevent oxygen diffusion. For experiments presented in Figs. 2(c)–2(f) and S11, bead rotation was recorded for 2 min in BMB with glucose in aerobic conditions, at which point the buffer was replaced with the pH-adjusted BMB. The slide was immediately sealed and recording continued for another 30 min. pH 5.5 buffer was adjusted with

a mixture of organic acids (0.9 mM acetate, 3.8 mM lactate, 1.4 mM formate and 0.45 mM succinate), whereas the rest of the buffers were pH adjusted using lactic acid only. The choice of the organic acid influences only the dynamics of the drop in motor speed [such as in Fig. 2(e)], and not the steady speed. The recording of motor speed was uninterrupted for the duration of the experiment (32 min). For alkaline shifts (Fig. 3), we recorded bead rotation for 2 min before flushing BMB adjusted with NaOH to pH 8.15 or 8.45. The slide was not sealed to allow another flush of BMB supplemented with 100 μM CCCP at 17 min and recording was continued for another 10 min. For experiments in Fig. S8 [10] motility buffer was prepared to the required pH by adjusting the K_2HPO_4 and KH_2PO_4 ratio and if needed with KOH. 40 mM potassium benzoate and 40 mM methylamine hydrochloride (PBMH) was used to equilibrate pH_e and pH_i [62]. The experimental protocol was simiar to [36]. Briefly, the tunnel slide was prepared in BMB of a given pH_e, PBMH was added 1 min before adding a given concentration of butanol and 1 min after the beginning of the speed recording. Butanol was then washed out 1 to 2 min later. Finally, PBMH was washed out and the sequence was repeated for each recording. The motor speed in PBMH was compared with the speed during butanol flush.

Relative (x, y) bead coordinates recorded with a position-sensitive detector were converted to the flagellar motor rotational frequencies by applying a flat-top discrete Fourier transform with 1.6384 s window and 0.1 s step size [36,43]. The resulting time series were median-filtered with the additional removal of 50 Hz ac frequency values and values below 10 Hz [36,43].

C. Intracellular pH measurements

The intracellular pH of the bacteria was measured with ratiometric pHluorin [40,75] using an established imaging protocol and sensor calibration [76]. Images were taken every 90 s with 50 ms exposure time.

Fluorescence images of pHluorin were analyzed as before [36,40]. An Otsu threshold followed by binary erosion and binary dilation was applied to both 475 nm and 395 nm excitation images, and the mean intensity was calculated for each cell in both channels. The ratio of these values with the background subtracted was later converted to pH units using a calibration curve generated following Ref. [40].

D. Intracellular ATP measurements

Cells were harvested at OD = 2, washed three times by centrifugation at 8000g for 2 min, and resuspended in BMB with 20 mM glucose, adjusted to pH 8.13–8.2 with KOH, and at final OD = 1. Cells were transferred to the Black Nunc 96-Well Plate (Flat Bottom), where 100 μM of CCCP was added with the multichannel pipette, simultaneously to all but one well, which served as a control. The measurements were performed using Biotek Synergy H1 plate reader, in 20, 60 s, or 5 min intervals post-CCCP addition, and on each well once (to avoid reported photoactivation of Queen 7 μM* [72]). Parallel measurements were performed with Wild type MG1655 to correct for background fluorescence by subtracting it from Queen7 μM* signal. To minimize photoactivation of neighboring wells in the plate reader measurements were repeated four times, and taken in a different well order. Cells were excited with 405 and 488 nm wavelengths, and emission was taken at 528 nm. The 405/488 ratios were converted to the ATP concentrations according to the calibration curve given. All experiments were performed at room temperature.

Queen7 μM* sensor calibration, Fig. S12(b) [10], was performed as before [72]. Cells were grown and prepared as before to Queen buffer [50 mM HEPES, 200 mM KCl, 1 mM $MgCl_2$, 0.05% Triton X-100, protease inhibitor cocktail (Sigma-Aldrich)] adjusted to pH 8.13. 100 μg/ml of lysozyme were added to the cells and incubated at room temperature for 15 min. The culture was then frozen to −70 °C and thawed twice to weaken the cell wall. Cells were later broken down by sonicating on ice at 4 °C with Qsonica Q700 at amplitude 50, four pulses of 30 s with 30 s interval (∼1000 J total energy input). Cell debris were spun down at 13000 g for 1 min and the supernatant was filtered with 0.22 μm syringe filter. Lysate fluorescence, containing Queen7 μM* and a known concentration of ATP (Adenosine 5'-triphosphate magnesium salt, Sigma-Aldrich), was measured at 405 and 488 nm excitation and 528 nm emission wavelengths. MG1655 lysate was used for background fluorescence measurements. The calibration curve was fitted with the sigmoid $y = (a1–a2)/(1 + e^{-k*[\log_{10}(x)-x0)]} + a2$, Fig. S12(b) [10].

E. Computational results

The computational algorithms, including useful heuristic approximations we developed, are described in the Supplemental Material [10]. To numerically solve the steady-state equations we used the MATLAB function VPASOLVE.

Our experimental data is available online [77].

ACKNOWLEDGMENTS

We would like to thank all members of the Pilizota and Swain labs as well as Sebastian Jaramillo-Riveri, Xavier Zaoui, Vincent Danos, Joshua Shaevitz, Terry Hwa, and Calin Guet for their support and useful discussions. We are particularly grateful to Ariel Amir for very detailed and thoughtful comments on the manuscript. We would like to thank Joanne Slonezewski and Linda Kenny for providing and helping us with reproducing their previously published data in Fig. S15. T.P., G.T., and E.K. were supported by the Human Frontier Science Program Grant No. RGP0041/2015, G.T. was supported by a PhD studentship from the Darwin Trust of Edinburgh, and PSS by the BBSRC Grant No. BB/W006545/1.

[1] T. A. Krulwich, G. Sachs, and E. Padan, Molecular aspects of bacterial pH sensing and homeostasis, Nat. Rev. Microbiol. **9**, 330 (2011).

[2] W. Aoi and Y. Marunaka, Importance of pH homeostasis in metabolic health and diseases: crucial role of membrane proton transport, BioMed Res. Int. **2014**, 598986 (2014).

[3] A.-S. Yang and B. Honig, On the pH dependence of protein stability, J. Mol. Biol. **231**, 459 (1993).

[4] J. M. Wood, Bacterial responses to osmotic challenges, J. Gen. Physiol. **145**, 381 (2015).

[5] D. C. Tosteson and J. F. Hoffman, Regulation of cell volume by active cation transport in high and low potassium sheep red cells, J. Gen. Physiol. **44**, 169 (1960).

[6] A. R. Kay, How cells can control their size by pumping ions, Front. Cell Dev. Biol. **5**, 41 (2017).

[7] D. A. Beard and H. Qian, *Chemical Biophysics: Quantitative Analysis of Chemical Systems* (Cambridge University Press, Cambridge, 2006).

[8] *Mathematical Physiology: I: Cellular Physiology*, edited by J. Keener and J. Sneyd, Interdisciplinary Applied Mathematics Vol. 8/1 (Springer, New York, NY, 2009).

[9] W.-C. Lo, E. Krasnopeeva, and T. Pilizota, Bacterial electrophysiology, Annu. Rev. Biophys. **53**, 487 (2024).

[10] See Supplemental Material at http://link.aps.org/supplemental/10.1103/PRXLife.2.043015 for additional figures, further details on the model and detailed information on our computational approaches.

[11] Y. Sowa and R. M. Berry, Bacterial flagellar motor, Q. Rev. Biophys. **41**, 103 (2008).

[12] D. Scott Cayley, H. J. Guttman, and M. T. Record, Biophysical characterization of changes in amounts and activity of *Escherichia coli* cell and compartment water and turgor pressure in response to osmotic stress, Biophys. J. **78**, 1748 (2000).

[13] Y. Deng, M. Sun, and J. W. Shaevitz, Direct measurement of cell wall stress stiffening and turgor pressure in live bacterial cells, Phys. Rev. Lett. **107**, 158101 (2011).

[14] E. Rojas, J. A. Theriot, and K. C. Huang, Response of escherichia coli growth rate to osmotic shock, Proc. Natl. Acad. Sci. USA **111**, 7807 (2014).

[15] L. Mancini, G. Terradot, T. Tian, Y. Y. Pu, Y. Li, C. J. Lo, F. Bai, and T. Pilizota, A general workflow for characterization of nernstian dyes and their effects on bacterial physiology, Biophys. J. **118**, 4 (2020).

[16] B. D. Bennett, E. H. Kimball, M. Gao, R. Osterhout, S. J. Van Dien, and J. D. Rabinowitz, Absolute metabolite concentrations and implied enzyme active site occupancy in *Escherichia coli*, Nat. Chem. Biol. **5**, 593 (2009).

[17] O. Boudker and G. Verdon, Structural perspectives on secondary active transporters, Trends Pharmacol. Sci. **31**, 418 (2010).

[18] A. L. Hodgkin and A. F. Huxley, A quantitative description of membrane current and its application to conduction and excitation in nerve, J. Physiol. **117**, 500 (1952).

[19] A. L. Hodgkin and A. F. Huxley, Currents carried by sodium and potassium ions through the membrane of the giant axon of loligo, J. Physiol. **116**, 449 (1952).

[20] K. D. Garlid, A. D. Beavis, and S. K. Ratkje, On the nature of ion leaks in energy-transducing membranes, Biochim. Biophys. Acta (BBA) **976**, 109 (1989).

[21] K. D. Garlid and P. Paucek, Mitochondrial potassium transport: the K^+ cycle, Biochim. Biophys. Acta (BBA) **1606**, 23 (2003).

[22] D. A. Beard and H. Qian, Relationship between thermodynamic driving force and one-way fluxes in reversible processes, PLoS ONE **2**, e144 (2007).

[23] P. Mitchell, Coupling of phosphorylation to electron and hydrogen transfer by a chemi-osmotic type of mechanism, Nature (London) **191**, 144 (1961).

[24] S. Chakraborty, R. S. Winardhi, L. K. Morgan, J. Yan, and L. J. Kenney, Non-canonical activation of OmpR drives acid and osmotic stress responses in single bacterial cells, Nat. Commun. **8**, 1587 (2017).

[25] C.-J. Lo, M. C. Leake, T. Pilizota, and R. M. Berry, Nonequivalence of membrane voltage and ion-gradient as driving forces for the bacterial flagellar motor at low load, Biophys. J. **93**, 294 (2007).

[26] T. Honda, J. Cremer, L. Mancini, Z. Zhang, T. Pilizota, and T. Hwa, Tight coordination of gene expression with cell size enables *Escherichia coli* to efficiently maintain motility across conditions, Proc. Natl. Acad. Sci. USA **119**, e2110342119 (2022).

[27] J. Cremer, T. Honda, Y. Tang, J. Wong-Ng, M. Vergassola, and T. Hwa, Chemotaxis as a navigation strategy to boost range expansion, Nature (London) **575**, 658 (2019).

[28] A. Accardi and C. Miller, Secondary active transport mediated by a prokaryotic homologue of ClC Cl-channels, Nature (London) **427**, 803 (2004).

[29] E. Pinner, E. Padan, and S. Schuldiner, Kinetic properties of NhaB, a Na^+/H^+ antiporter from *Escherichia coli*, J. Biol. Chem. **269**, 26274 (1994).

[30] D. Taglicht, E. Padan, and S. Schuldiner, Proton-sodium stoichiometry of NhaA, an electrogenic antiporter from *Escherichia coli*, J. Biol. Chem. **268**, 5382 (1993).

[31] J. Slonczewski, M. Fujisawa, M. Dopson, and T. A. Krulwich, Cytoplasmic pH measurement and homeostasis in bacteria and archaea, Adv. Microbial Physiol. **55**, 1 (2009).

[32] S. Schuldiner and H. Fishkes, Sodium-proton antiport in isolated membrane vesicles of escherichia coli, Biochemistry **17**, 706 (1978).

[33] H. Richard and J. W. Foster, *Escherichia coli* glutamate- and arginine-dependent acid resistance systems increase internal pH and reverse transmembrane potential, J. Bacteriol. **186**, 6032 (2004).

[34] J. H. Kaplan, Biochemistry of Na, K-ATPase, Annu. Rev. Biochem. **71**, 511 (2002).

[35] Y. V. Morimoto, S. Kojima, K. Namba, and T. Minamino, M153R mutation in a pH-sensitive green fluorescent protein stabilizes its fusion proteins, PLoS ONE **6**, e19598 (2011).

[36] E. Krasnopeeva, C.-J. Lo, and T. Pilizota, Single-cell bacterial electrophysiology reveals mechanisms of stress-induced damage, Biophys. J. **116**, 2390 (2019).

[37] E. Krasnopeeva, U. E. Barboza-Perez, J. Rosko, T. Pilizota, and C.-J. Lo, Bacterial flagellar motor as a multimodal biosensor, Methods **193**, 5 (2021).

[38] D. C. Fung and H. C. Berg, Powering the flagellar motor of *Escherichia coli* with an external voltage source, Nature (London) **375**, 809 (1995).

[39] C. V. Gabel and H. C. Berg, The speed of the flagellar rotary motor of *Escherichia coli* varies linearly with protonmotive force, Proc. Natl. Acad. Sci. USA **100**, 8748 (2003).

[40] Y. K. Wang, E. Krasnopeeva, S.-Y. Lin, F. Bai, T. Pilizota, and C.-J. Lo, Comparison of *Escherichia coli* surface attachment methods for single-cell microscopy, Sci. Rep. **9**, 19418 (2019).

[41] G. Kuwajima, Construction of a minimum-size functional flagellin of *Escherichia coli*, J. Bacteriol. **170**, 3305 (1988).

[42] W. S. Ryu, R. M. Berry, and H. C. Berg, Torque-generating units of the flagellar motor of *Escherichia coli* have a high duty ratio, Nature (London) **403**, 444 (2000).

[43] J. Rosko, V. Martinez, W. Poon, and T. Pilizota, Osmotaxis in *Escherichia coli* through changes in motor speed, Proc. Natl. Acad. Sci. USA **114**, E7969 (2017).

[44] K. Svoboda, C. F. Schmidt, B. J. Schnapp, and S. M. Block, Direct observation of kinesin stepping by optical trapping interferometry, Nature (London) **365**, 721 (1993).

[45] W. Denk and W. W. Webb, Optical measurement of picometer displacements of transparent microscopic objects, Appl. Opt. **29**, 2382 (1990).

[46] R. Buda, Y. Liu, J. Yang, S. Hegde, K. Stevenson, F. Bai, and T. Pilizota, Dynamics of *Escherichia coli's* passive response to a sudden decrease in external osmolarity, Proc. Natl. Acad. Sci. USA **113**, E5838 (2016).

[47] J. Schwarz-Linek, J. Arlt, A. Jepson, A. Dawson, T. Vissers, D. Miroli, T. Pilizota, V. A. Martinez, and W. C. K. Poon, *Escherichia coli* as a model active colloid: A practical introduction, Colloids Surfaces B: Biointerf. **137**, 2 (2016).

[48] R. I. Macey, J. S. Adorante, and F. W. Orme, Erythrocyte membrane potentials determined by hydrogen ion distribution, Biochim. Biophys. Acta (BBA) **512**, 284 (1978).

[49] P. Bennekou and P. Christophersen, Flux ratio of valinomycin-mediated K^+ fluxes across the human red cell membrane in the presence of the protonophore CCCP, J. Membr. Biol. **93**, 221 (1986).

[50] B. Z. Cavari and Y. Avi-Dor, Effect of carbonyl cyanide m-chlorophenylhydrazone on respiration and respiration-dependent phosphorylation in *Escherichia coli*, Biochem. J. **103**, 601 (1967).

[51] D. Le, E. Krasnopeeva, F. Sinjab, T. Pilizota, and M. Kim, Active efflux leads to heterogeneous dissipation of proton motive force by protonophores in bacteria, mBio **12**, doi:10.1128/mbio.00676-21 (2021).

[52] D. Zilberstein, V. Agmon, S. Schuldiner, and E. Padan, *Escherichia coli* intracellular pH, membrane potential, and cell growth, J. Bacteriol. **158**, 246 (1984).

[53] R. Iyer, T. M. Iverson, A. Accardi, and C. Miller, A biological role for prokaryotic ClC chloride channels, Nature (London) **419**, 715 (2002).

[54] E. Padan, The enlightening encounter between structure and function in the NhaA Na^+H^+ antiporter, Trends Biochem. Sci. **33**, 435 (2008).

[55] E. Padan, E. Bibi, M. Ito, and T. A. Krulwich, Alkaline pH homeostasis in bacteria: New insights, Biochim. Biophys. Acta (BBA) **1717**, 67 (2005).

[56] D. Taglicht, E. Padan, and S. Schuldiner, Overproduction and purification of a functional Na^+/H^+ antiporter coded by nhaA (ant) from *Escherichia coli*, J. Biol. Chem. **266**, 11289 (1991).

[57] U. Kanjee and W. A. Houry, Mechanisms of acid resistance in *Escherichia coli*, Annu. Rev. Microbiol. **67**, 65 (2013).

[58] E. Pennacchietti, F. Giovannercole, and D. De Biase, Acid survival mechanisms in neutralophilic bacteria, in *Stress and Environmental Regulation of Gene Expression and Adaptation in Bacteria* (John Wiley & Sons, New York, 2016), pp. 911–926.

[59] J. Lin, M. P. Smith, K. C. Chapin, H. S. Baik, G. N. Bennett, and J. W. Foster, Mechanisms of acid resistance in enterohemorrhagic *Escherichia coli*, Appl. Environm. Microbiol. **62**, 3094 (1996).

[60] J. L. Slonczewski, R. M. Macnab, J. R. Alger, and A. M. Castle, Effects of pH and repellent tactic stimuli on protein methylation levels in *Escherichia coli*, J. Bacteriol. **152**, 384 (1982).

[61] J. C. Wilks and J. L. Slonczewski, pH of the cytoplasm and periplasm of *Escherichia coli*: Rapid measurement by green fluorescent protein fluorimetry, J. Bacteriol. **189**, 5601 (2007).

[62] K. A. Martinez, R. D. Kitko, J. P. Mershon, H. E. Adcox, K. A. Malek, M. B. Berkmen, and J. L. Slonczewski, Cytoplasmic pH response to acid stress in individual cells of *Escherichia coli* and Bacillus subtilis observed by fluorescence ratio imaging microscopy, Appl. Environm. Microbiol. **78**, 3706 (2012).

[63] S. Chakraborty and L. J. Kenney, A new role of OmpR in acid and osmotic stress in Salmonella and *E. coli*, Front. Microbiol. **9**, 2656 (2018).

[64] C. Baker-Austin and M. Dopson, Life in acid: pH homeostasis in acidophiles, Trends Microbiol. **15**, 165 (2007).

[65] D. McLaggan, M. Keyhan, and A. Matin, Chloride transport pathways and their bioenergetic implications in the obligate acidophile bacillus coagulans, J. Bacteriol. **172**, 1485 (1990).

[66] T. A. Krulwich, J. Liu, M. Morino, M. Fujisawa, M. Ito, and D. B. Hicks, *Adaptive Mechanisms of Extreme Alkaliphiles* (Springer Japan, Tokyo, 2011), pp. 119–139.

[67] D. G. Fuster and R. T. Alexander, Traditional and emerging roles for the SLC9 Na^+/H^+ exchangers, Pflügers Archiv: Eur. J. Physiol. **466**, 61 (2014).

[68] M. Schwede, K. Garbett, K. Mirnics, D. H. Geschwind, and E. M. Morrow, Genes for endosomal NHE6 and NHE9 are misregulated in autism brains, Mol. Psych. **19**, 277 (2014).

[69] M. Schushan, M. Xiang, P. Bogomiakov, E. Padan, R. Rao, and N. Ben-Tal, Model-guided mutagenesis drives functional studies of human NHA2, implicated in hypertension, J. Mol. Biol. **396**, 1181 (2010).

[70] P. G. Vallés, V. Bocanegra, A. G. Lorenzo, and V. V. Costantino, Physiological functions and regulation of the Na^+/H^+ exchanger [NHE1] in renal tubule epithelial cells, Kidney Blood Pressure Res. **40**, 452 (2015).

[71] Y. Ishida, S. Nayak, J. A. Mindell, and M. Grabe, A model of lysosomal pH regulation, J. Gen. Physiol. **141**, 705 (2013).

[72] L. Mancini and T. Pilizota, Environmental conditions define the energetics of bacterial dormancy and its antibiotic susceptibility, Biophys. J. **122**, 3207 (2023).

[73] T. Pilizota, J. Rosko, and E. Krasnopeeva, BFM speed recording with back-focal-plane interferometry, 10.17504/protocols.io.bch2it8e, March 2021.

[74] U. B. Perez, E. Krasnopeeva, J. Rosko, and T. Pilizota, Tunnel slide preparation for motor speed recordings, 10.17504/protocols.io.bcjdiui6, March 2021.

[75] G. Miesenböck, D. A. De Angelis, and J. E. Rothman, Visualizing secretion and synaptic transmission with pH-sensitive green fluorescent proteins, Nature (London) **394**, 192 (1998).

[76] E. Krasnopeeva and T. Pilizota, Cytoplasmic pH measurements with pHluorin, 10.17504/protocols.io.bhi7j4hn, March 2021.

[77] https://datashare.is.ed.ac.uk/handle/10283/2058